Results in Physics 29 (2021) 104655

Contents lists available at ScienceDirect

Results in Physics

journal homepage: www.elsevier.com/locate/rinp

Symmetries in cavity models: Beyond the rotating wave approximation

Gilberto Medeiros Nakamura [a,b], Tiago José Arruda [c], Alexandre Souto Martinez [d,e,*]

[a] Université Paris-Saclay, CNRS/IN2P3, IJCLab, 91405 Orsay, France
[b] Université de Paris, IJCLab, 91405 Orsay, France
[c] Instituto de Ciências Exatas (ICEx), Universidade Federal de Alfenas (UNIFAL), 37133-840 Alfenas, Minas Gerais, Brazil
[d] Faculdade de Filosofia, Ciências e Letras de Ribeirão Preto (FFCLRP), Universidade de São Paulo (USP), Avenida Bandeirantes 3900, 14040-901, Ribeirão Preto, São Paulo, Brazil
[e] Instituto Nacional de Ciência e Tecnologia - Sistemas Complexos (INCT-SC), Brazil

ARTICLE INFO

Keywords:
Algebraic methods
Quantum mechanics
Quantum optics
Cooperative phenomena in quantum optical systems
Optical angular momentum and its quantum aspects
Cavity quantum electrodynamics

ABSTRACT

The interaction of confined atoms with a single mode radiation field is the main subject in the theory of cavity quantum electrodynamics. The constraints imposed by the cavity on matter and radiation fields give rise to collective phenomena. One possible outcome is the enhanced and coherent spontaneous emission of photons by the atoms: the superradiance. As predicted by Dicke, conservation laws are essential in superradiance and are derived from the matter-interaction Hamiltonian. Here, we consider N two-level ultracold atoms interacting with a single mode bosonic field, in the Dicke Hamiltonian, and trapped inside a non-dissipative optical cavity. Numerical and analytical results derived from finite size regime indicate the matter–radiation coupling strength, λ, is insufficient to draw the complete picture of the system. Instead, they support the relevance of $U(1)$ symmetry, which prompts the study of (i) particle and angular momentum conservation, (ii) the constraints imposed to correlation functions and (iii) the influence of symmetries in the system dynamics. Further exploring the $U(1)$ and rotational symmetries permits a simple interpretation of antirotating contributions as spin–orbit operators. As application, we show two species of ultracold clouds develop interactions due to antirotating operators.

Introduction

Interference is a crucial phenomenon to tailor optical response of nanoscale systems [1–3] and lies in the foundation of quantum theories. It becomes even more relevant when short range interactions are strong and shape the system dynamics [4]. Examples are readily available in condensed matter physics such as quantum dots [5], metallic nanoparticles [6] and nanostructures [7]. Quantum interference is also an integral part of quantum information theory [8,9] and the study of ultracold atoms [10,11]. In particular, the aorecited physical systems are known to share at least one superradiant phase. Superradiance is the collective phenomenon where N particles confined inside an optical cavity spontaneously emit coherent light. The shared electromagnetic field inside the cavity produces interatomic correlations [12], provided the typical distance between atoms is smaller than the emitted photon wavelength [13–15]. In this regime, the spontaneous photon emission does not occur as N independent events, even for small N, as verified by recent experiments [16]. This collective behaviour emerges from fluctuations which further develop a large positive feedback [17]. For non-pumped systems, the characteristic cavity photo-emission is a sharp pulse, with duration $\tau_{sr} = \tau_{sp}/N$, where τ_{sp} is the standard spontaneous decay time, and intensity proportional to N^2 [14,18], which is one hallmark of the superradiance effect.

Central to any discussion regarding cavity models is the inclusion of antirotating operators. The nomenclature antirotating (or counter-rotating) is derived from the rotating wave approximation (RWA), where the rapid oscillations in the interaction picture are neglected, providing an extensive simplification to the interpretation of particle absorption–emission process [19]. However, there is enough evidence supporting that the antirotating terms cannot be discarded [20]. As demonstrated in Ref. [21], the entanglement among qubits undergoes a discontinuity due to the antirotating operators. When the RWA is in place, there is no such observation. Beyond the RWA, an exact solution for all arbitrary coupling is available in the thermodynamic limit using the Holstein–Primakoff transformations [22,23], which allows the identification of quantum phase transitions and chaotic regimes. For finite N, only numerical solutions are available for the whole coupling

* Corresponding author at: Faculdade de Filosofia, Ciências e Letras de Ribeirão Preto (FFCLRP), Universidade de São Paulo (USP), Avenida Bandeirantes 3900, 14040-901, Ribeirão Preto, São Paulo, Brazil.
E-mail addresses: nakamura@ijclab.in2p3.fr (G.M. Nakamura), tiago.arruda@unifal-mg.edu.br (T.J. Arruda), asmartinez@usp.br (A.S. Martinez).

https://doi.org/10.1016/j.rinp.2021.104655
Received 5 July 2021; Accepted 4 August 2021
Available online 28 August 2021

range [24]. As such, several analytical techniques have been introduced along the years to mitigate the RWA while still keeping its convenient absorption–emission interpretation [9,25–28].

Despite the experimental and theoretical advances in the study of cavity models, particle and angular momentum conservation are often neglected subjects. Here we study the symmetries present in the Dicke Hamiltonian for a finite number of two-level atoms, at zero temperature and without dissipation, where both particle and momentum conservation are crucial. The motivation is quite simple: the matter–radiation interaction is conservative and relies on bilinear operator products [29]. Yet, it exhibits neither explicit photon number nor atomic excitation conservation. However, the electric charge inside the cavity is a conserved quantity and, thus, the model is $U(1)$ invariant. The existence of such conserved quantity has subtle ramifications: the average contribution of antirotating operators vanishes for suitable first kind gauge transformations, as we demonstrate in this research. This property may also be used to evaluate the mean energy, reducing the procedure to the minimization of functional equations with constraints. The other relevant symmetry we considered is the conservation of angular momentum. The underlying conservation law defines a set of Lie operators sharing one common parameter, the photon cutoff number l. In the finite regime, the matter–radiation interaction unfolds as a combination of spin–orbit interactions. As an application, we study the interference among two distinct and non-interacting gas clouds sharing the same non-dissipative optical cavity. The constraints imposed by the cavity, electric charge and angular momentum conservation allow us to explicitly unveil the interaction between both gas clouds. This property enables the interference among the atomic clouds and heavily depends on antirotating operators, therefore neglected under RWA.

The scheme of Fig. 1 illustrates the underlying physical processes described by the Dicke model. Let H be the Dicke Hamiltonian that describes matter–radiation interaction:

$$H = \hbar\omega a^\dagger a + \Omega J^z + \lambda(a + a^\dagger)(J^- + J^+), \tag{1}$$

where $[a, a^\dagger] = 1$ for single bosonic field operators trapped in the optical cavity, with ω being the frequency of the cavity mode; $J^\alpha = \sum_{k=1}^{N} J_k^\alpha$ ($\alpha = z, \pm$) and J_k^z corresponds to the energy level operator for each particle ($k = 1, \dots, N$); the Lie operators J_k^α satisfy $[J_m^+, J_n^-] = 2\hbar J_m^z \delta_{mn}$ and $[J_m^z, J_n^\pm] = \pm\hbar J_m^\pm \delta_{mn}$. Due to the above algebraic relations, the detuned energy difference between two atomic levels is $\Delta E = \hbar\Omega$, i.e., Ω is the resonance frequency of the atoms. Radiation and matter operators, as usual, commute with each other, $[a, J_k^\alpha] = [a^\dagger, J_k^\alpha] = 0$, for any k and α. The matter–radiation interaction is expressed by the last parcel in the right-hand side of Eq. (1), quantified by the coupling λ. The interaction is Hermitian and contains two distinct contributions. The first contribution is the so-called antirotating term, $a^\dagger J_k^+ + a J_k^-$, often misunderstood as the non-conservative interaction while the opposite holds for the rotating term, $a J_k^+ + a^\dagger J_k^-$. The puzzling non-conservative aspect of antirotating operators arises from the duality of local two-level operators J_k: they share mixed fermionic and bosonic rules, $\{J_k^\alpha, J_k^\beta\} = (\hbar^2/4)\delta_{\alpha,-\beta}$ and $[J_k^\alpha, J_{k'}^\beta] = 0$, for $k \neq k'$. This severely impairs the particle absorption–emission interpretation as the particles under consideration are neither fermions nor bosons [30,31]. The same phenomenon is a common occurrence in condensed matter problems, where suitable algebraic transformations are used to select only one behaviour. Obviously, if cavity losses are neglected, the Hamiltonian does not depend explicitly on time and thus conserves the total probability and also energy.

This paper is organized as follows. In Section "Finite size effects", we report numerical results for finite number of atoms N, at resonant frequency $\omega = \Omega$. Finite size effects are discussed and it is shown their characterization depends on both coupling strength λ and number of photons stored in the cavity. In Section "$U(1)$ symmetry", the latter are used as supporting evidence to investigate the electric charge conservation and $U(1)$ symmetry. Gauge invariance is then employed to determine the constraint which the system must abide and its implications to the equations of motion. This constraint allow us to introduce finite angular momentum operators in Section "Angular operators". Finally, in Section "Two atomic species", we employ our formalism to a cavity model describing the interference between non-interacting ultracold gas clouds, composed by two distinct atomic species.

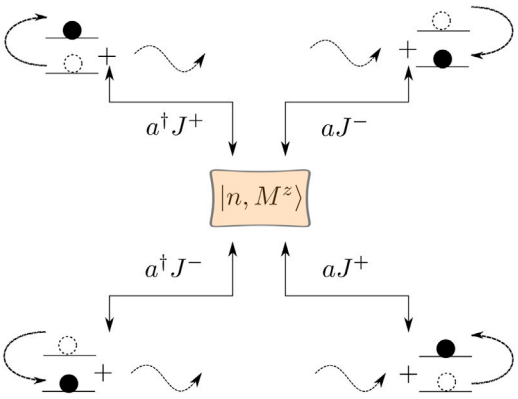

Fig. 1. Matter–radiation interaction in the Dicke model. A state with n photons and $M^z + N/2$ excited atoms undergoes four different process: atomic excitation (decay) and photon absorption (emission) ; atomic decay (excitation) and photon absorption (emission). One disregards operators aJ_k^- and $a^\dagger J_k^+$ in the rotating wave approximation. This approximation eliminates both off diagonal and diagonal operators whenever H^2 is concerned, thus removing corrections to energy and correlations. Examples may be found even for simple diagonal operators such as $(a^\dagger J_k^+ + aJ_k^-)^2 = 2a^\dagger a J_k^+ J_k^- - a^\dagger a + J^+ J + 1$.

Finite size effects

Macroscopic properties are often described by atomic and photon densities, N/V and $\langle n\rangle/V$, respectively. The thermodynamic limit is reached when both ratios have well defined values as the volume $V \to \infty$. In this regime, extensive quantities scale with both mean number of photons, $\langle n\rangle$, and mean number of atoms in the excited state, $\langle J^z/\hbar + N/2\rangle$, trapped inside the cavity. This observation agrees with general thermodynamic guidelines. However, the finite regime also stores interesting non-trivial physical properties and are the main focus of research areas such as quantum information and nanotechnology. These properties are derived from finite size effects, which are non-extensive corrections to extensive quantities. In this section, we introduce the physical scales to measure the finite size effects within the Dicke model, which ultimately allow us to investigate its symmetry content.

For very large photon density, the radiation field inside the cavity remains nearly unchanged in the limit $N/V \to 0$ and, thus, is described by coherent states $|\gamma\rangle$. Under these assumptions, the Hamiltonian in Eq. (1) takes a much simpler form: $H_{\rm ch} = \hbar\omega|\gamma|^2 + \Omega J^z + 2\lambda\,\mathrm{Re}(\gamma)(J^- + J^+)$, i.e, N disjoint two-level operators, each with eigenenergies $E_\pm = \pm(\hbar\Omega/2)\sqrt{1 + 16\mathrm{Re}(\gamma)^2(\lambda/\Omega)^2}$. Hence, the eigenspectrum is obtained by combining $E_\pm$ for N atoms, which may be used to compute the partition function $Z(T)$, at a given temperature T. However, the crucial information to be learn here is that the mean photon density $\langle n\rangle/V = |\gamma|^2/V$ remains unchanged.

The remaining case occurs when the average photon density also vanishes in the thermodynamic limit, $\langle n\rangle/V \to 0$. In this regime, finite size effects are expected to produce relevant corrections. Therefore, to investigate them, one must first reduce or limit the average number of photons in the cavity. One may consider an adiabatic process where one photon is removed from the cavity, while kept at very low temperatures, $T \to 0$. If the process is iterated, the assumption that the radiation fields are well described by coherent states no longer holds. The assumption breaks when $\langle n\rangle$ approaches $\langle J^z/\hbar + N/2\rangle$

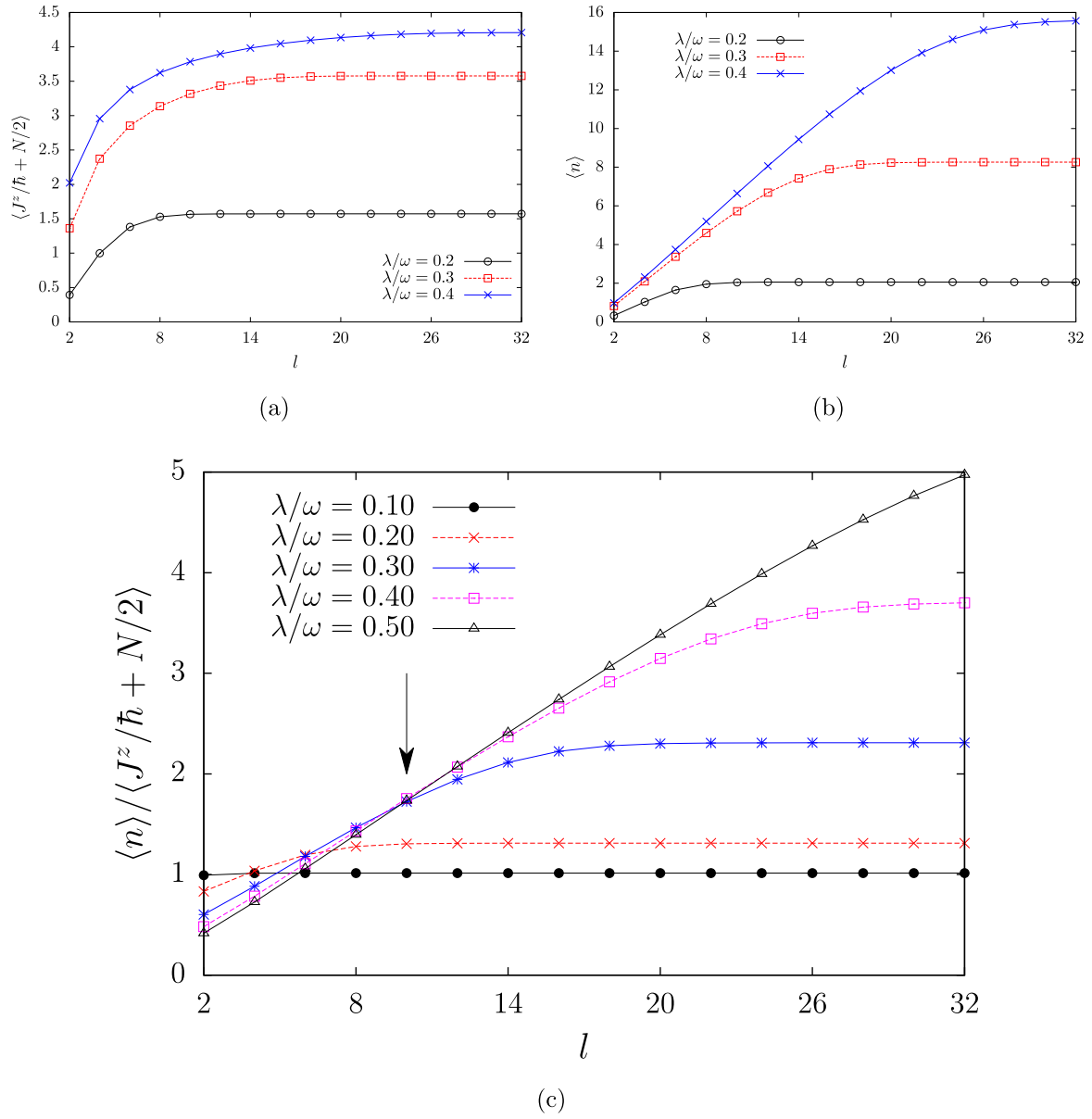

Fig. 2. Finite size effects. Number of excited atoms $\langle J^z/\hbar + N/2\rangle$ and the mean number of photons $\langle n\rangle$ for the ground state in the Dicke model, in (a) and (b), respectively, against photon cutoff l. Corrections due to finite l are observable for both quantities, approaching constant values, at distinct rates, at the critical photon cutoff $l_c(\lambda)$ for each coupling λ. In (c), the arrow shows the ratio $r_N(\lambda, l) = \langle n\rangle/\langle J^z/\hbar + N/2\rangle \equiv r$ develops a crossing point at the line $l = N$ for any $\lambda > \lambda_c$, below which $\partial r/\partial\lambda = 0$ and strongly suppress finite size effects.

as a continuous function of matter–radiation coupling λ. The same result is obtained if one introduces an explicit photon cutoff, l, for photon number inside the cavity, as done numerically in Ref. [32]. This procedure is equivalent to truncate the Fock space, allowing the study of finite size effects on lower energy levels. It is important to mention that states with higher energies often contains more photons and are more susceptible to the photon cutoff. In light of the above consideration, we restrict the following analysis to the lowest energy levels, with strong emphasis on the ground state.

With the photon cutoff in place, one studies the average number of photons, $\langle n\rangle$, evaluated in the ground state as a function of l and λ, for fixed N, ω and Ω. By varying l while keeping λ fixed, one finds the value l_c above which any increase in l keeps the photon density unchanged. Similar behaviour is expected for $\langle J^z/\hbar + N/2\rangle$ as well, since matter fields are coupled to radiation fields. Fig. 2 displays numerical results for both $\langle J^z/\hbar + N/2\rangle$ and $\langle n\rangle$ with $\lambda/\omega = m/10$ ($m = 2, 3, 4$) and $N = 10$.

For $l \gg N$, both average number of photons and average number of excited atoms are expected to assume constant values. Thus, the ratio $r_N(\lambda, l) = \langle n\rangle/\langle J^z/\hbar + N/2\rangle$ also acquires constant value and is used to identify the physical regime. In what follows, the analysis is centred at the photon cutoff $l = N$, where finite size effects are expected to be relevant, since the maximum number of photons in the Fock space is equal to the number of atoms. In accordance with our previous argument, corrections due to finite number of photon are expected for increasing λ and $l \to N$. In fact, numerical results obtained from exact diagonalization of Eq. (1) show there exists a coupling value λ_c, at $l = N$ plane, above which $r_N(\lambda \geqslant \lambda_c, l = N) \equiv r_c(N)$ and depends only on N as Fig. 2 illustrates. Thus, λ_c demarks two distinct behaviours for the ground state with $l = N$. In the first region, $\lambda < \lambda_c$, the ground state is insensitive to non-extensive corrections due to the finite number of photons; in the second region, finite effects are relevant.

Note that these results were obtained for finite $N \sim o(10^1)$ since the computational code performs the numerical diagonalization of Eq. (1)

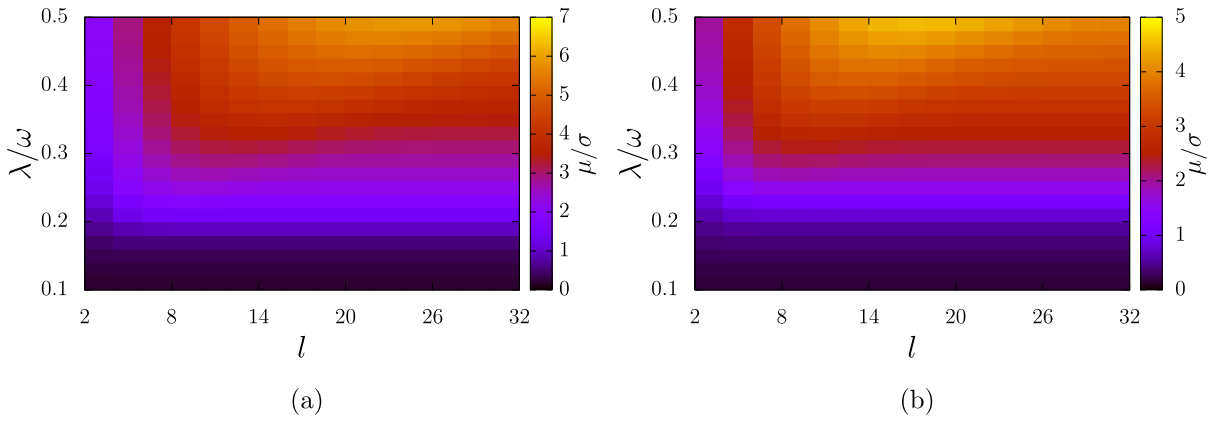

Fig. 3. Noise-to-signal. In (a), the ground state signal-to-noise ratio μ/σ is shown with $N = 10$. At small matter–radiation coupling $\lambda \to 0$, the lowest eigenenergy $E_0 = -\hbar\Omega N/2$ is independent on $\langle n\rangle$ and the ground state exhibits strong resistance towards finite size corrections. For large coupling values, $\lambda > \lambda_c$, μ/σ develops positive gradient with increasing l and λ, thus requiring large l to minimize surface effects. In (b), $N = 8$ and similar behaviour is observed.

while the Fock space grows as $l \times 2^N$. Nevertheless, inspired by our previous result, we define λ_c as the coupling value where $r_N(\lambda, l = N)$ is maximum, $\partial r_N/\partial\lambda_c = 0$. In what follows, the Fock space is organized in a particular way to provide a simpler picture of ground state properties. Let the integer $\nu = 0, \ldots, l \times 2^N - 1$ be the index for each vector $|\phi_\nu\rangle$ such that the ground state is $|\psi_0\rangle = \sum_\nu c_\nu|\phi_\nu\rangle$, with $\nu = \alpha + h^m$, h is the dimension of atomic Hilbert space, $\alpha = 0, \ldots, h-1$ and $m = 0, \ldots, l-1$. Under this data organization scheme, the number of photons increases by one every h vectors. In addition, let $\mu = \sum_\nu \nu|c_\nu|^2$ and $\sigma^2 = \sum_\nu(\nu-\mu)^2|c_\nu|^2$ be the ground state mean index and variance, respectively. Increments in $\langle n\rangle$ are related to increments in μ; similarly, increments of σ^2 are related to variations in both mean number of photons and mean number of excited atoms. At the particular case $l = N$, the ground state is insensitive to finite size effects for $\lambda < \lambda_c$ and, hence, the signal-to-noise ratio, μ/σ, also follows the same behaviour, as Fig. 3 illustrates.

For $\lambda > \lambda_c$, μ/σ increases either due to increasing μ or decreasing σ, which case requires the introduction of the Fano factor, $F_N(\lambda, l) = \sigma^2/\mu \equiv F$, also known as dispersion index. Fig. 4 shows F possess a maximum for $l \geqslant N$ at $\lambda = \lambda_c$. Furthermore, F is insensitive to finite size effects as long as $l \geqslant N$ and $\lambda < \lambda_c$, in agreement with our previous result. However, it also describes three regions with distinct characteristics. In the first region , R_1, Fano factor is a rapid decreasing function of λ, suggesting strong finite size corrections; in the second region, R_2, F still decreases with λ but at slower rates than in R_1, creating large plateaus for $l \gg N$. Thus, in R_2 the shape of ground state probability distribution remains approximately constant with varying λ.

$U(1)$ symmetry

Despite λ_c being defined via ground state, all remaining eigenstates $|\psi_k\rangle$ and eigenenergies E_k exhibit corrections due to the finitude of photon cutoff l. To investigate the complete eigenspectrum, it is convenient to further examine the discrete symmetries present in Eq. (1), particularly those concerning the atomic states. This is performed by the cyclic permutation operator, T, which acts over atomic states. For instance, let $|\uparrow\downarrow\cdots\downarrow\rangle$ represent an atomic configuration with N atoms, one of which is excited and indicated by the symbol $\uparrow$. The action of T over $|\uparrow\downarrow\cdots\downarrow\rangle$ is $T|\uparrow\downarrow\cdots\downarrow\rangle = |\downarrow\uparrow\downarrow\cdots\downarrow\rangle$. The eigenvectors $|\uparrow\downarrow\cdots\downarrow, p\rangle$ of T are constructed as linear combination, $|\uparrow\downarrow\cdots\downarrow, p\rangle = (1/N_p)\sum_{k=0}^{N-1}(e^{2\imath\pi p/N}T)^k|\uparrow\downarrow\cdots\downarrow\rangle$, holding the permutation quantum number $p = 0, \ldots, N-1$. The normalization factor is N_p and the eigenvalue equation reads $T|\uparrow\downarrow\cdots\downarrow, p\rangle = e^{-2\imath\pi p/N}|\uparrow\downarrow\cdots\downarrow, p\rangle$. The generalization for additional excited atoms is straightforward.

Since the operators $J^{\pm,z}$ are symmetric under permutations, they also commute with T, $\left[J^{\pm,z}, T\right] = 0$, meaning the Hamiltonian in Eq. (1) may be put in block diagonal form, one block or sector for each p. In particular, the ground state $|\psi_0\rangle$ is found at $p = 0$ sector. Fig. 5 displays the energy spectrum within the $p = 0$ sector and the unfolding of additional symmetries with non-vanishing matter–radiation interaction and increasing photon cutoff l. Finite size effects due to finite photon cutoff are readily shown by the energy difference $\Delta E(\lambda) = E_1(\lambda) - E_0(\lambda)$, where E_0 and $E_1(\lambda)$ are the energies of ground and the first excited states within the same permutation sector, respectively, as show in Fig. 6. Accordingly, there exists a finite energy gap $\Delta E(\lambda < \lambda_c) > 0$, which is independent of l, for $l > N$. For $\lambda > \lambda_c$ the model develops finite size corrections as the first energy gap vanishes.

In the vanishing λ limit, Eq. (1) conserves both mean number of photons $\langle n\rangle$ and number of excited atoms $\langle J^z/\hbar + N/2\rangle$, which is translated into the $U(1) \otimes U(1)$ symmetry or independent particle conservation. However, for non-vanishing λ, this picture does not hold as the ratio $\langle n\rangle/\langle J^z/\hbar + N/2\rangle$ depends on the ratio λ/ω. To examine this claim, consider the action of Eq. (1) in the strong coupling regime $\lambda \gg \omega = \Omega$ on the entropic state

$$|\psi\rangle = \left[\prod_{\otimes}^{N} \frac{|\uparrow\rangle - |\downarrow\rangle}{\sqrt{2}}\right] \otimes \left[\frac{\sum_{m=0}^{l}|m\rangle}{\sqrt{l+1}}\right]. \tag{2}$$

It is a straightforward task to compute the following inequalities:

$$-2\hbar\lambda N l^{1/2} \leqslant \langle\psi|\lambda(a^\dagger + a)(J^+ + J^-)|\psi\rangle \leqslant -\hbar\lambda N l^{1/2}, \tag{3}$$

which produce $-2\hbar\lambda N l^{1/2} \leqslant \langle\psi|H|\psi\rangle - \hbar\omega l/2 \leqslant -\hbar\lambda N l^{1/2}$ and whose extremal condition occurs at $N(\lambda/\omega)^2 \leqslant 2\langle n\rangle/N \leqslant 4N(\lambda/\omega)^2$.

The apparent dependence of $\langle J^z\rangle$ on $\langle n\rangle$ is further clarified from the viewpoint of the unitary transformation $U(\theta) = \exp[\imath\theta\left(a^\dagger a - N/2 + J^z/\hbar\right)]$. Under the $U(1)$ symmetry, both matter and radiation fields modify themselves coherently, due to the cavity constraint, creating a conserved charge q. We now address the existence of an additional global $U(1)$ symmetry in Eq. (1). For simplicity sake, let us firstly consider the non-interacting scenario in Eq. (1). The Hamiltonian clearly admits $U(1) \otimes U(1)$ symmetry for vanishing λ, namely,

$$J_k^\pm \to e^{\mp\imath\phi}J_k^\pm, \quad a \to e^{\imath\theta}a, \tag{4}$$

where the real phases ϕ and θ label the gauge transformations of first kind for atomic and the respective radiation field. These transformations maintain both radiation and matter algebras unchanged. At same time, the foundation of both operators lies in the electromagnetic theory and, as such, the first kind gauge invariance ultimately translate into charge conservation. Since the fields are non-interacting, the charge is independently conserved for each field.

For $\lambda \neq 0$, however, there exists interaction between the atomic electric dipole and radiation field. In absence of relativistic effects and high energy photons, anti-matter creation is negligible and electric

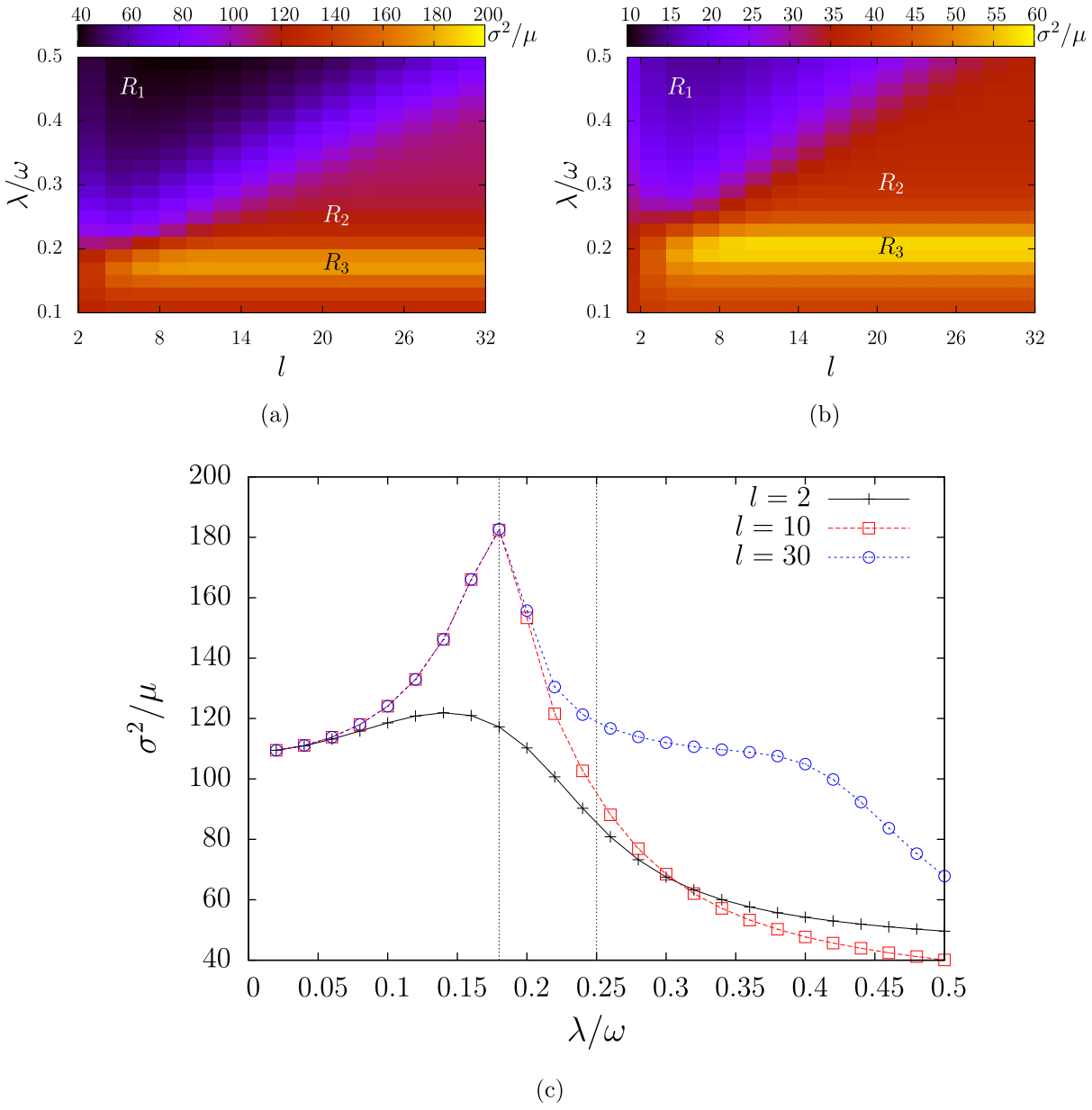

Fig. 4. Fano factor $F_N(\lambda, l)$ for ground state. In (a) $N = 10$ while (b) $N = 8$ atoms. Both share three distinguishable regions: R_1 (R_3), where finite size effects are dominant (irrelevant); and the intermediate region R_2 where F_N is a slow decreasing function of λ, i.e., an increase in μ is followed by similar increase in variance σ^2, creating a plateau. (c) shows the Fano factor with $N = 10$ and $l = 2, 10, 30$. The dotted line indicates λ_c where F_N develops a maximum. For $l \geqslant N$ and $\lambda < \lambda_c$, ground state properties are not affected by photon cutoff l.

charge conservation is tied to both fields. This requirement introduces mutual dependence of matter gauge ϕ with radiation gauge θ, i.e., $\phi \equiv \phi(\theta)$. This relation breaks down the $U(1) \otimes U(1)$ symmetry to $U(1)$, leading to additional constraints the Dicke model must satisfy. The Hamiltonian in Eq. (1) under the transformations of Eq. (4) reads

$$H = H_0 + \lambda \sum_k^N \left(a J_k^+ \mathrm{e}^{\imath(\theta - \phi(\theta))} + \mathrm{hc} \right) + \lambda \sum_k^N \left(a J_k^- \mathrm{e}^{\imath(\theta + \phi(\theta))} + \mathrm{hc} \right). \tag{5}$$

Here $H_0 = \hbar\omega a^\dagger a + \Omega J^z$ is the diagonal contribution. The energy spectrum in $p = 0$ sector is shown in Fig. 7, normalized by the maximum energy stored by the field in the cavity, for varying photon gauge parameter θ. As expected, the energy spectrum is gauge invariant since physical observables should not depend on any particular gauge choice θ or $\phi(\theta)$. This observation may be used to design additional constraints to simplify the evaluation of physical observables, including the antirotating contributions to energies.

The two most convenient observables are the mean number of photons, $\langle a^\dagger a \rangle$, and the mean atomic magnetization, $\langle J^z \rangle$, which are naturally invariant by gauge transformations of first kind. The gauge invariance constraints are set by $(d/d\theta)\langle a^\dagger a \rangle = (d/d\theta)\langle J^z \rangle = 0$. These constraints are applied to both equations of motion, $\imath\hbar(d/dt)\langle O \rangle = \langle [O, H] \rangle$, with $O = a^\dagger a, J^z$. The results are

$$-\frac{\hbar}{\lambda}\frac{d}{d\theta}\frac{d}{dt}\langle a^\dagger a \rangle = 0 = \sum_{k=1}^N \left\langle \left(1 + \frac{d\phi}{d\theta}\right)\left(a J_k^- \mathrm{e}^{\imath(\theta+\phi)} + a^\dagger J_k^+ \mathrm{e}^{-\imath(\theta+\phi)}\right)\right\rangle + \sum_{k=1}^N \left\langle \left(1 - \frac{d\phi}{d\theta}\right)\left(a J_k^+ \mathrm{e}^{\imath(\theta-\phi)} + a^\dagger J_k^- \mathrm{e}^{-\imath(\theta-\phi)}\right)\right\rangle. \tag{6}$$

$$-\frac{1}{\lambda}\frac{d}{d\theta}\frac{d}{dt}\langle J^z \rangle = 0 = \sum_{k=1}^N \left\langle \left(1 + \frac{d\phi}{d\theta}\right)\left(a J_k^- \mathrm{e}^{\imath(\theta+\phi)} + a^\dagger J_k^+ \mathrm{e}^{-\imath(\theta+\phi)}\right)\right\rangle - \sum_{k=1}^N \left\langle \left(1 - \frac{d\phi}{d\theta}\right)\left(a J_k^+ \mathrm{e}^{\imath(\theta-\phi)} + a^\dagger J_k^- \mathrm{e}^{-\imath(\theta-\phi)}\right)\right\rangle. \tag{7}$$

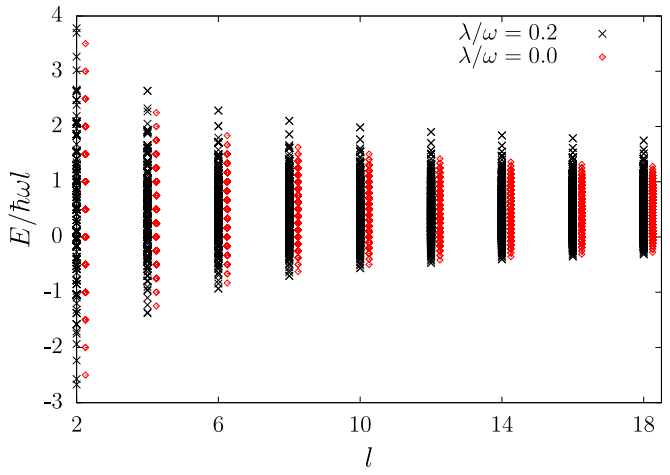

Fig. 5. Degeneracy. Normalized energy spectrum for $N = 10$ atoms ($\Omega = \omega$) for varying photon number cutoff l, in the permutation sector $p = 0$. The red diamonds are the energies in the non-interacting regime, $\lambda/\omega = 0$, and are offset by δl for clarity sake. In this regime, the normalized lowest (highest) energy level is $E_{\mp}/\hbar\omega l = \mp(N/2l)+(1\mp1)/2$. The black crosses show the normalized energy levels for $\lambda/\omega = 1/5$. The matter–radiation interaction lifts degeneracy and shifts the density of energy levels towards the lowest level for increasing l, resulting in non-trivial mean photon occupation.

These equations set up suitable gauge choices for matter and radiation operators. In fact, an illuminating correlation function is uncovered and related to the RWA when $d\phi/d\theta = 1$:

$$\sum_{k=1}^{N}\langle aJ_k^- e^{2i\theta} + a^\dagger J_k^+ e^{-2i\theta}\rangle = 0. \tag{8}$$

Setting $\theta = m\pi$, $m = 0, \pm1, \ldots$, is equivalent to state that the RWA is accurate if and only if there is no correlation or interference among the atoms and radiation composing the ensemble. It is amusing that even though RWA imposes such a severe restriction on the system, antirotating operators provide null contribution when averaged over the ensemble, which explains the general validity and broad applicability of RWA. The other simple gauge choice, which will not be considered in this study, is $d\phi/d\theta = -1$. It states the total energy is gauge invariant and continuously flows back and forth from field to matter, with opposite rates. Nonetheless, the constraint in Eq. (8) should always be employed whenever antirotating operators are concerned, despite their trivial average contribution to energy.

One useful property is obtained from energy equations: the constraint Eq. (8) changes the energy eigenvalue equation into a functional minimization problem. Let $|\varphi_r\rangle$ be an eigenstate of the Hamiltonian H, subjected to the RWA, with eigenvalue E_r^{RWA}. If the linear combination $|\psi\rangle = \sum_r c_r|\varphi_r\rangle$, with associated density matrix ρ, satisfies Eq. (8), then the energy equation reduces to $\mathrm{Tr}\left[\rho\left(H - H^{\mathrm{RWA}}\right)\right] = 0$, which is an energy functional equation for the solution ρ, $\langle E\rangle = \sum_r E_r^{\mathrm{RWA}}\rho_{rr}$.

Angular operators

The atomic effects mediated by the radiation field are most evident when one considers the effects and constraints imposed by global rotation. For that purpose, the operators in Eq. (1) require additional transformations to exhibit rotational content and must preserve the permutation quantum number p. We start considering the case where $0 \le n \le l$ photons are confined inside the optical cavity without atoms, $N = 0$. In this scenario, the net physical angular momentum is $\Delta m = \hbar n$ and the energy is $E = \hbar\omega n$. The complete energy spectrum is derived by varying $n = 0, 1, \ldots, l$; the eigenstates correspond to the basis of orbital momentum operator, $|l, m\rangle$, with $m = -l, -l+1, \ldots, +l$. This simple model permits the identification $q = l$ as the total angular momentum eigenvalue while $q_z = m$ is the z-projected eigenvalue. These results must be generalized to non-vanishing N. For that purpose, one make extensive use of Holstein–Primakoff transformations [33] and define the conserved charge $q_z = \langle Q^z\rangle/\hbar$, whose associated operators are

$$Q^z \equiv L^z + J^z, \tag{9}$$

$$Q^+ \equiv L^+ + J^+, \tag{10}$$

$$Q^- \equiv L^- + J^-, \tag{11}$$

with $L^+ = \hbar\sqrt{l+1-a^\dagger a}\,a^\dagger$ and $L^z = \hbar(2a^\dagger a - l)$. The operator L^- is obtained by the usual Hermitian conjugation. Here l is the cutoff value for number of photons trapped inside the cavity for each bosonic mode. Under this assumption, one obtains $[Q^+, Q^-] = 2\hbar Q^z$ and $[Q^z, Q^\pm] = \pm\hbar Q^\pm$. Moreover, the Jacobi identity is satisfied, $[Q^z,[Q^+,Q^-]]+[Q^-,[Q^z,Q^+]]+[Q^+,[Q^-,Q^z]] = 0$, thus defining a compact Lie algebra. The algebraic machinery constructed so far encourages the interpretation of Q^z as the z-projected angular momentum operator. Therefore, radiation operators are interpreted as orbital angular momentum operators, while matter analogue plays the role of spin. Both claims naturally lead to the definition of Casimir operator $Q^2 = (Q^z)^2 + (1/2)\{Q^+, Q^-\}$. It is worth mentioning, the finite photon cutoff leads naturally to the Holstein–Primakoff transformations to photon fields, instead of atomic fields as usually done.

Finite size corrections due to the finite photon cutoff l occurs in Eqs. (9)–(11) after the linearization procedure,

$$L^+ = \hbar\sqrt{l+1}\left(1 - \frac{a^\dagger a}{2l+2}\right)a^\dagger + o(l^{-3/2}). \tag{12}$$

Up to order l^{-1}, one may compute the inverse operator $[1 - a^\dagger a/(l+1)]^{-1/2} = 1 + a^\dagger a/2(l+1) + o(l^{-2})$. It allows one to rewrite the bosonic operators $a^\dagger$ and a using the orbital counterparts, L^+ and L^-, respectively. This results provides an elucidating interpretation for both rotating and antirotating contributions: they are expressed as spin–orbit operators, which naturally favour the eigenstates of Casimir operator. Further analysis leads to two important results. First, rotating operators are diagonal:

$$aJ^+ + a^\dagger J^- \approx \frac{1}{\hbar\sqrt{l+1}}\left[\left(Q^2 - (Q^z)^2 - 2L^zJ^z\right)\left(1 + \frac{l}{4(l+1)} + \frac{L^z}{2\hbar(l+1)}\right)\right]. \tag{13}$$

It reflects the simplicity of rotating operators and their contributions, in agreement with earlier claim that RWA is unable to account for interference phenomena. The second result is that antirotating operators produce non-diagonal contributions:

$$a^\dagger J^\dagger + aJ \approx \frac{2}{\hbar\sqrt{l+1}}\left[\left(L^xJ^x - L^yJ^y\right)\left(1 + \frac{l}{4(l+1)} + \frac{L^z}{2\hbar(l+1)}\right)\right], \tag{14}$$

which, unlike Eq. (13), couples different sectors of q_z for a given q eigenvalue.

Two atomic species

One model which allows the investigation of particle and rotational symmetries is the system composed by two distinct atomic species $\xi = 1, 2$, confined within a high-quality optical cavity, as illustrated in Fig. 8. Each ensemble holds N_ξ two-level atoms that only interact with their respective bosonic modes, characterized by photons with energy $\hbar\omega_\xi$ and spin $m_\xi = (-1)^{\xi-1}$. In short, the cavity holds two two-level atomic species and two bosonic polarized modes. Since polarization is taken in account, atomic transitions for each ensemble satisfy strict selection rules. Again, as in the case studied in Section "Angular operators", the cavity imposes strong constraints on matter and radiation fields within its boundaries. Here, the shared electromagnetic field couples both atomic ensembles, which would otherwise be non-interacting in open environments. Interference occurs when both gas clouds are brought together, with interactions mediated by quantized

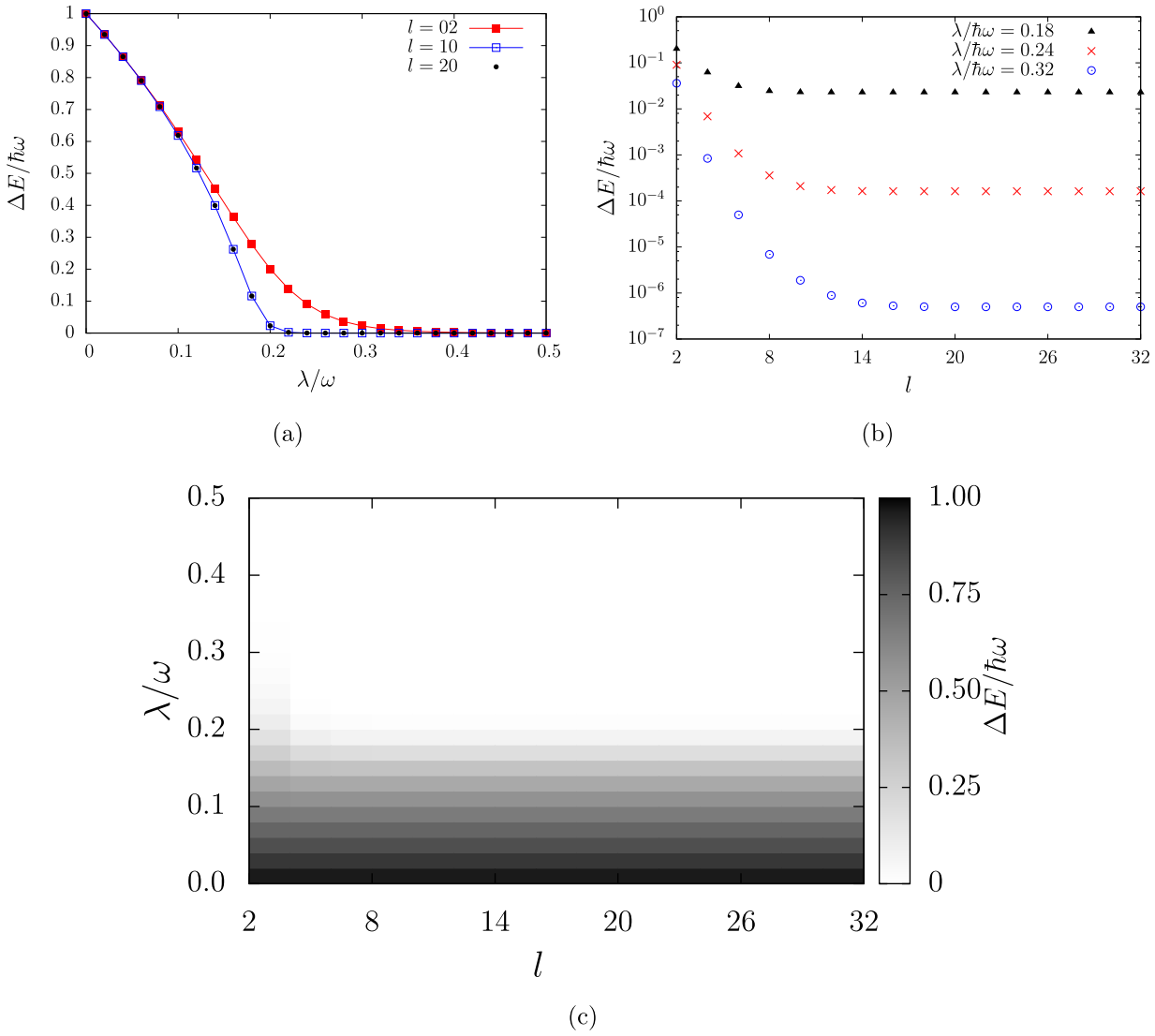

Fig. 6. Energy gap. First energy gap for $N = 10$ atoms ($\Omega = \omega$) for varying photon number cutoff l, in the permutation sector $p = 0$. In (a), the photon number cutoff is fixed and additional corrections are not observed with $l \geqslant N$ and $\lambda < \lambda_c$. (b) At λ_c, the first energy gap decreases exponentially with λ and l. (c) $\Delta E/\hbar\omega$ colourmap at $p = 0$ sector. λ_c is the coupling that separates finite ΔE phase from exponentially degenerate ground states.

and confined radiation fields, as long as the system and cavity remain coherent for long time intervals. The interference among the atomic clouds are most evident when one considers the constraints imposed by $U(1)$ and rotational symmetries, as we show in what follows.

So far, the $U(1)$ symmetry has been considered for a single atomic species. When both gas clouds are present, the superposition of electromagnetic fields inside the optical cavity couples both parameters $\theta_{1,2}$. This is a necessary condition to ensure the conservation of electric charge in the theory. Therefore, the gauge parameters satisfy $\theta_1 = \theta_2 = \theta$. This unique feature dictates that the density operator for each gas cloud are not separable as one would expect: Eq. (8) for each ensemble are coupled by the shared gauge parameter θ. For instance, given the density matrix ρ_1' associated with the ensemble $\xi = 1$, one might try to find a suitable θ' as solution of Eq. (8). To obtain the complete solution, one would then solve Eq. (8), with fixed θ', for the density matrix ρ_2' associated with ensemble $\xi = 2$. Thus, solutions obtained from Eq. (8) for one atomic species restrict the configuration state for the other atomic species.

As in the previous case, we start by considering the case where $0 \leq n_\xi \leq l$ photons are confined inside the optical cavity without atoms, $N_1 = N_2 = 0$, producing net physical angular momentum $\Delta m = \hbar(n_1 - n_2)$ and energy $E = \hbar\omega_1 n_1 + \hbar\omega_2 n_2$. Again, one identifies $q = l$ and $q_z = \Delta m$ as the total angular momentum eigenvalue and the z-projected eigenvalue, respectively. These results are generalized to non-vanishing N_ξ using Eqs. (6) and (7), for both gas clouds. The natural choice (and often used) would be $q_z = \sum_\xi \langle a_\xi^\dagger a_\xi + J_\xi^z/\hbar\rangle$. However, this option is only viable while using the RWA, in agreement with Eq. (8), as it disregards correlations among atoms in either the same or distinct ensembles. The Holstein–Primakoff transformations [33] are employed again with charge $q_z = \langle Q^z\rangle/\hbar$. The rotation generators are

$$Q^z \equiv \hbar(a_1^\dagger a_1 - a_2^\dagger a_2) + J_1^z - J_2^z, \tag{15}$$

$$Q^+ \equiv L_{1,l}^+ + L_{2,l}^- + J_1^+ + J_2^-, \tag{16}$$

$$Q^- \equiv L_{1,l}^- + L_{2,l}^+ + J_1^- + J_2^+. \tag{17}$$

where $L_{1,l}^+ = \hbar\sqrt{l + 1 - a_1^\dagger a_1}\, a_1^\dagger$ and $L_{2,l}^- = \hbar a_2\sqrt{l + 1 - a_2^\dagger a_2}$. Eqs. (15)–(17) provide the same algebraic structure as in the single specie case, leading to interpretation of Q^z as projected angular momentum operator and $Q^2 = (Q^z)^2 + (1/2)\{Q^+, Q^-\}$ as the Casimir operator.

The new Hilbert space and Q operators are natural candidates to study the interference between two gas clouds in the superradiant regime. The superradiant phase is characterized by large amounts of

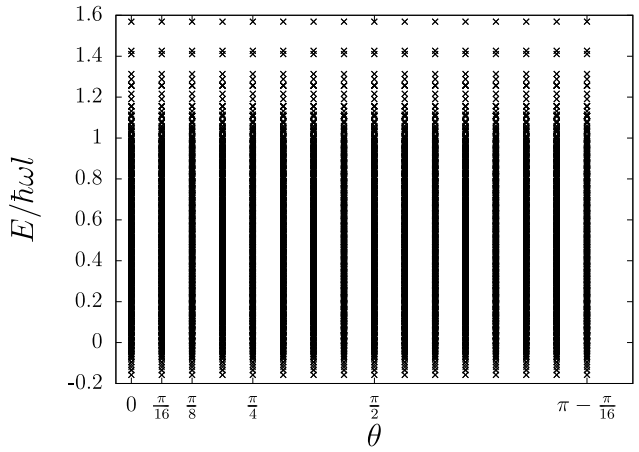

Fig. 7. Gauge invariance. Normalized eigenspectra for several gauge values θ with $N = 8$ atoms, photon cutoff $l = 32$, $\lambda/\omega = 1/4$ and permutation sector $p = 0$. Changes in gauge parameter θ produces no observable modifications in the energy spectrum, evidencing the gauge invariance of first kind.

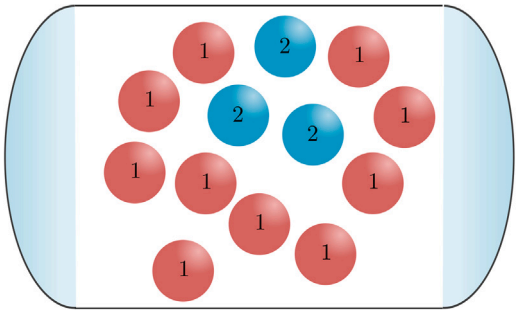

Fig. 8. Two distinct two-level atomic ensembles inside an high-quality optical cavity. Each kind of atom is labelled by the integer $\xi = 1, 2$ and interact only with their respective radiation fields. For $\xi = 1$, atoms only absorb photons with energy $\hbar\omega_1$ and spin $m = +1$ while atoms with $\xi = 2$ absorbs photons with energy $\hbar\omega_2$ and spin $m = -1$. Each atomic ensemble holds N_ξ atoms.

energy stored in matter fields, which is coherently discharged as a short pulse. For a non-dissipative cavity, this also implies the energy available from electromagnetic sources are lower than those in non-superradiant phases. Thus, the photon number n_ξ is expected to be much smaller than the photon cutoff value l, with ratio $\delta n_\xi = \langle a_\xi^\dagger a_\xi\rangle/l \ll 1$. This observation justifies the linearization of Holstein–Primakoff transformations for arbitrary values of N_ξ, since the relevant expansion parameter is the shared cutoff value l. Within this approximation, the linearized orbital momentum operator $L_{1,l}^+$ up to first order in $l^{-1/2}$ is

$$L_{1,l}^+ \approx \hbar\sqrt{l+1}\left(1 - \frac{a_1^\dagger a_1}{2l+2}\right)a_1^\dagger. \tag{18}$$

Analogous expansions are obtained for the remaining ladder operators $L_{\xi,l}^\pm$.

Up to order l^{-1}, one may compute the inverse operator $[1 - a_\xi^\dagger a_\xi/(l+1)]^{-1/2} = 1 + a_\xi^\dagger a_\xi/2(l+1) + o(l^{-2})$. It allows one to rewrite the bosonic operators $a_\xi^\dagger$ and a_ξ using the orbital counterparts, $L_{\xi,l}^+$ and $L_{\xi,l}^-$, respectively. Again, the rotating and antirotating contributions are interpreted as spin–orbit operators. However, their action now connects the time evolution of two atomic species *via* the shared electromagnetic field even though the atoms themselves do not interact with each other.

Due to the conservation of q_z and q, the antirotating contributions now require the employment of Q^2 operator and its associated eigenspace. This condition mix both atomic states, which in turn permits the interference among the distinct gas clouds. For instance, consider the case where the system is initially found in the configuration containing one superradiant cloud and one completely discharged, both with N atoms. For simplicity sake, let us additionally consider N photons with spin $m = -1$ are available inside the cavity. This particular configuration is represented as $|N, 0; 0, N\rangle$ with $q_z = 0$. After a time interval t, one may measure the state $|0, N; N, 0\rangle$. The state $|0, 0; 0, 0\rangle$ also carries $q_z = 0$ and can be measured as well. While the former event is expected within the RWA framework, including the simple quantum emission–absorption, the latter is the regular outcome in the quantum angular theory. Energy is conserved since the Casimir and spin–orbit operators commute with each other. In fact, Eq. (8) tell us antirotating operators produce vanishing contributions to energy. Their role is to ensure all states with same q are also accounted to the action of rotating operators.

The operator Q^z defined in Eq. (15) is $U(1)$ invariant while the operators $Q^\pm$ in Eqs. (16) and (17) introduce correlations among the distinct ensembles due to the shared cutoff parameter, l. These definitions, however, are not unique: if photons with energy $\hbar\omega_1$ and $\hbar\omega_2$ are uncorrelated, then there exists a set of operators $\tilde{Q}^z = Q^z + \hbar(l_2 - l_1)$ and $\tilde{Q}^+ = \hbar(l_1 + 1 - a_1^\dagger a_1)^{1/2}a_1^\dagger + \hbar a_2(l_2 + 1 - a_2^\dagger a_2)^{1/2} + J_1^+ + J_2^-$, which also satisfies the same algebraic relations. Indeed, the $\tilde{Q}$ operators reproduce the local conservation of angular momenta for two non-interacting ensembles, both matter and radiation field, each trapped in their respective optical cavity. Since each one possesses local q conservation, they also do not interfere.

Conclusion

We have shown the role played by conservation laws in diatomic cavity models. The $U(1)$ symmetry, despite its simplicity, imposes severe restrictions to correlation functions. At same time, it enforces the antirotating operators must produce vanishing contributions to energy to preserve the electromagnetic charge in the theory. The constraints are also used to produce a functional energy equation for the density matrix. This fact is reinforced when conservation of total angular momentum is imposed. In such case, the matter–radiation interaction is expressed as the spin–orbit interaction and uncovers the implicit interaction between two apparently non-interacting gas clouds. The interference between them occurs only due to the antirotating contributions. Of course, the requirement of conservation of angular momentum is not always feasible: cavities are subjected to losses, either by transmitting light, thermal photonic generation and, ultimately, coherence. Coherent radiation losses implemented via Lindblad operators would be required to satisfy the first kind gauge invariance, leading to a dissipative version of Eq. (8). At same time, it would add a torque-like feature to the equations of motion, thus enabling transitions between states with differing q.

CRediT authorship contribution statement

Gilberto Medeiros Nakamura: Conceptualization, Data curation, Formal analysis, Funding acquisition, Investigation, Methodology, Project administration, Resources, Software, Validation, Visualization, Writing – original draft, Writing – review & editing. **Tiago José Arruda:** Conceptualization, Data curation, Formal analysis, Funding acquisition, Investigation, Methodology, Project administration, Validation, Visualization, Writing – original draft, Writing – review & editing. **Alexandre Souto Martinez:** Conceptualization, Data curation, Formal analysis, Funding acquisition, Investigation, Methodology, Project administration, Resources, Software, Supervision, Validation, Visualization, Writing – original draft, Writing – review & editing.

Declaration of competing interest

The authors declare that they have no known competing financial interests or personal relationships that could have appeared to influence the work reported in this paper.

Acknowledgements

We are grateful to F.A. Pinheiro and G.C. Cardoso for clarifying discussions and comments, which inspired the numerical analysis reported in this research. The authors also acknowledge the Brazilian agencies for support. T.J.A. holds grants from FAPESP 2015/21194-3 and A.S.M. holds grants from CNPq 309851/2018-1.

References

[1] Arruda TJ, Martinez AS, Pinheiro FA. Unconventional Fano effect and off-resonance field enhancement in plasmonic coated spheres. Phys Rev A 2013;87:043841. http://dx.doi.org/10.1103/PhysRevA.87.043841.

[2] Arruda TJ, Martinez AS, Pinheiro FA. Tunable multiple Fano resonances in magnetic single-layered core–shell particles. Phys Rev A 2015;92:023835. http://dx.doi.org/10.1103/PhysRevA.92.023835.

[3] Arruda TJ, Martinez AS, Pinheiro FA, Bachelard R, Slama S, Courteille PW. Chap. Fano resonances in plasmonic core–shell particles and the Purcell effect. In: Fano Resonances in Optics and Microwaves: Physics and Applications. Switzerland: Springer Cham; 2018, p. 445–72.

[4] Kozub M, Pawicki L, Machnikowski P. Enhanced spontaneous optical emission from inhomogeneous ensembles of quantum dots is induced by short-range coupling. Phys Rev B 2012;86:121305. http://dx.doi.org/10.1103/PhysRevB.86.121305.

[5] Scheibner M, Schmidt T, Worschech L, Forchel A, Bacher G, Passow T, Hommel D. Superradiance of quantum dots. Nat Phys 2007;3:106–10. http://dx.doi.org/10.1038/nphys494.

[6] Pustovit VN, Shahbazyan TV. Cooperative emission of light by an ensemble of dipoles near a metal nanoparticle: The plasmonic Dicke effect. Phys Rev Lett 2009;102:077401. http://dx.doi.org/10.1103/PhysRevLett.102.077401.

[7] Teperik TV, Degiron A. Superradiant optical emitters coupled to an array of nanosize metallic antennas. Phys Rev Lett 2012;108:147401. http://dx.doi.org/10.1103/PhysRevLett.108.147401.

[8] Rotondo P, Cosentino Lagomarsino M, Viola G. Dicke simulators with emergent collective quantum computational abilities. Phys Rev Lett 2015;114:143601. http://dx.doi.org/10.1103/PhysRevLett.114.143601.

[9] Sornborger AT, Cleland AN, Geller MR. Superconducting phase qubit coupled to a nanomechanical resonator: Beyond the rotating-wave approximation. Phys Rev A 2004;70:052315. http://dx.doi.org/10.1103/PhysRevA.70.052315.

[10] Hofferberth S, Fischer B, Schumm T, Schmiedmayer J, Lesanovsky I. Ultracold atoms in radio-frequency dressed potentials beyond the rotating-wave approximation. Phys Rev A 2007;76:013401. http://dx.doi.org/10.1103/PhysRevA.76.013401.

[11] Baden MP, Arnold KJ, Grimsmo AL, Parkins S, Barrett MD. Realization of the dicke model using cavity-assisted Raman transitions. Phys Rev Lett 2014;113:020408. http://dx.doi.org/10.1103/PhysRevLett.113.020408.

[12] Dicke RH. Coherence in spontaneous radiation processes. Phys Rev 1954;93:99–110. http://dx.doi.org/10.1103/PhysRev.93.99.

[13] Gross M, Haroche S. Superradiance: An essay on the theory of collective spontaneous emission. Phys Rep 1982;93:301–96, http://dx.doi.org/10.1016/0370-1573(82)90102-8.

[14] Kaluzny Y, Goy P, Gross M, Raimond JM, Haroche S. Observation of self-induced Rabi oscillations in two-level atoms excited inside a resonant cavity: The ringing regime of superradiance. Phys Rev Lett 1983;51:1175–8. http://dx.doi.org/10.1103/PhysRevLett.51.1175.

[15] Skribanowitz N, Herman IP, MacGillivray JC, Feld MS. Observation of Dicke superradiance in optically pumped HF gas. Phys Rev Lett 1973;30:309–12. http://dx.doi.org/10.1103/PhysRevLett.30.309.

[16] Mlynek JA, Abdumalikov AA, Eichler C, Wallraff A. Observation of Dicke superradiance for two artificial atoms in a cavity with high decay rate. Nature Commun 2014;5. http://dx.doi.org/10.1038/ncomms6186.

[17] Yukalov VI, Yukalova EP. Dynamics of quantum dot superradiance. Phys Rev B 2010;81:075308. http://dx.doi.org/10.1103/PhysRevB.81.075308.

[18] Bonifacio R, Schwendimann P, Haake F. Quantum statistical theory of superradiance. I. Phys Rev A 1971;4:302–13. http://dx.doi.org/10.1103/PhysRevA.4.302.

[19] Hepp K, Lieb EH. On the superradiant phase transition for molecules in a quantized radiation field: the Dicke maser model. Ann Phys, NY 1973;76:360–404, http://dx.doi.org/10.1016/0003-4916(73)90039-0.

[20] Knight PL, Allen L. Rotating-wave approximation in coherent interactions. Phys Rev A 1973;7:368–70. http://dx.doi.org/10.1103/PhysRevA.7.368.

[21] Jing J, Lü Z-G, Ficek Z. Breakdown of the rotating-wave approximation in the description of entanglement of spin-anticorrelated states. Phys Rev A 2009;79:044305. http://dx.doi.org/10.1103/PhysRevA.79.044305.

[22] Emary C, Brandes T. Quantum chaos triggered by precursors of a quantum phase transition: The Dicke model. Phys Rev Lett 2003;90:044101. http://dx.doi.org/10.1103/PhysRevLett.90.044101.

[23] Brandes T. Excited-state quantum phase transitions in Dicke superradiance models. Phys Rev E 2013;88:032133. http://dx.doi.org/10.1103/PhysRevE.88.032133.

[24] Chen Q-H, Zhang Y-Y, Liu T, Wang K-L. Numerically exact solution to the finite-size Dicke model. Phys Rev A 2008;78:051801. http://dx.doi.org/10.1103/PhysRevA.78.051801.

[25] Irish EK. Generalized rotating-wave approximation for arbitrarily large coupling. Phys Rev Lett 2007;99:173601. http://dx.doi.org/10.1103/PhysRevLett.99.173601.

[26] Zheng H, Zhu SY, Zubairy MS. Quantum Zeno and anti-Zeno effects: Without the rotating-wave approximation. Phys Rev Lett 2008;101:200404. http://dx.doi.org/10.1103/PhysRevLett.101.200404.

[27] Scully MO. Collective Lamb shift in single photon Dicke superradiance. Phys Rev Lett 2009;102:143601. http://dx.doi.org/10.1103/PhysRevLett.102.143601.

[28] Li Y, Evers J, Feng W, Zhu S-Y. Spectrum of collective spontaneous emission beyond the rotating-wave approximation. Phys Rev A 2013;87:053837. http://dx.doi.org/10.1103/PhysRevA.87.053837.

[29] Werlang T, Dodonov AV, Duzzioni EI, Villas-Bôas CJ. Rabi model beyond the rotating-wave approximation: Generation of photons from vacuum through decoherence. Phys Rev A 2008;78:053805. http://dx.doi.org/10.1103/PhysRevA.78.053805.

[30] Nakamura GM, Mulato M, Martinez AS. Spin gap in coupled magnetic layers. Physica A 2016;451:313–9, https://doi.org/10.1016/j.physa.2016.01.070.

[31] Alcaraz FC, Nakamura GM. Phase diagram and spectral properties of a new exactly integrable spin-1 quantum chain. J Phys A: Math Gen 2010;43:155002, http://stacks.iop.org/1751-8121/43/i=15/a=155002.

[32] Emary C, Brandes T. Chaos and the quantum phase transition in the Dicke model. Phys Rev E 2003;67:066203. http://dx.doi.org/10.1103/PhysRevE.67.066203.

[33] Holstein T, Primakoff H. Field dependence of the intrinsic domain magnetization of a ferromagnet. Phys Rev 1940;58:1098–113. http://dx.doi.org/10.1103/PhysRev.58.1098.